PLOS | ONE

RESEARCH ARTICLE

Graphite Carbon-Supported Mo_2C Nanocomposites by a Single-Step Solid State Reaction for Electrochemical Oxygen Reduction

K. Huang[1], K. Bi[1], C. Liang[1], S. Lin[1], W. J. Wang[2]*, T. Z. Yang[2], J. Liu[3], R. Zhang[1], D. Y. Fan[1], Y. G. Wang[1], M. Lei[1]*

1 State Key Laboratory of Information Photonics and Optical Communications & School of Science, Beijing University of Posts and Telecommunications, Beijing, China, **2** Beijing National Laboratory for Condensed Matter Physics, Institute of Physics, Chinese Academy of Sciences, Beijing, China, **3** School of Materials Science and Engineering, Central South University, Changsha, Hunan, China

* wjwang@iphy.ac.cn (WJW); minglei@bupt.edu.cn (ML)

Citation: Huang K, Bi K, Liang C, Lin S, Wang WJ, Yang TZ, et al. (2015) Graphite Carbon-Supported Mo_2C Nanocomposites by a Single-Step Solid State Reaction for Electrochemical Oxygen Reduction. PLoS ONE 10(9): e0138330. doi:10.1371/journal.pone.0138330

Editor: Jason B. Love, University of Edinburgh, UNITED KINGDOM

Received: May 8, 2015

Accepted: August 28, 2015

Published: September 18, 2015

Data Availability Statement: All relevant data are within the paper.

Funding: This work was financially supported by The National Basic Research Program of China (Grant No. 2013CB932901), Program for New Century Excellent Talents in University (NCET-13-0684), Fund of State Key Laboratory of Information Photonics and Optical Communications (Beijing University of Posts and Telecommunications, P. R. China), and National Natural Science Foundation of China (Grant nos. 61376018,61377097,51102019, 61177085, 51272031,51472033). The funders had no role in

Abstract

Novel graphite-molybdenum carbide nanocomposites (G-Mo_2C) are synthesized by a typical solid state reaction with melamine and MoO_3 as precursors under inert atmosphere. The characterization results indicate that G-Mo_2C composites are composed of high crystallization and purity of Mo_2C and few layers of graphite carbon. Mo_2C nanoparticles with sizes ranging from 5 to 50 nm are uniformly supported by surrounding graphite layers. It is believed that Mo atom resulting from the reduction of MoO_3 is beneficial to the immobilization of graphite carbon. Moreover, the electrocatalytic performances of G-Mo_2C for ORR in alkaline medium are investigated by cyclic voltammetry (CV), rotating disk electrode (RDE) and chronoamperometry test with 3M methanol. The results show that G-Mo_2C has a considerable catalytic activity and superior methanol tolerance performance for the oxygen reduction reaction (ORR) benefiting from the chemical interaction between the carbide nanoparticles and graphite carbon.

Introduction

As is well known to all, ORR is the main performance-limiting factor due to its sluggish kinetics in the high-efficiency energy conversion devices such as fuel cells and metal-air batteries [1–15]. To accelerate the ORR process, precious Pt-based electrocatalysts are highly desired, but the limited reserve and increasing price of Pt have been turned out to be great restrictions of such devices [16–18]. Fortunately, due to the recent advancements in anion-exchange membrane materials [19–22], the serious CO_2-poisoning problem to KOH electrolyte which will reduce the ionic conductivity of the electrolyte and block the pores in the electrode has been overcome. In addition, considering the superior kinetics of the ORR in alkaline solution to that

study design, data collection and analysis,decision to publish, or preparation of the manuscript.

Competing Interests: The authors have declared that no competing interests exist.

in acidic media, a much wider range of less expensive materials can be used as efficient and stable ORR catalysts in alkaline solution [23–25].

On the other hand, transition metal carbides such as molybdenum carbide and tungsten carbide owning the properties of covalent solids, ionic crystals and transition metals have been proved to own similar electronic and catalytic performances to Pt-group noble metals in reactions such as hydrogenation, dehydrogenation and isomerization of hydrocarbons [26–28]. Recently, Wan et al. synthesized multiple phases of molybdenum carbide as electrocatalysts for hydrogen evolution reaction (HER) and showed promise as an alternative to Pt [29]. Ma et al. modified molybdenum carbide by nickel using a temperature-programmed reaction process and used it for steam reforming of methanol as enhanced catalysts [30]. Yan and coworkers loaded Pt on Mo_2C particles through ionic exchange process with a synergistic effect and strong interaction force for methanol electro-oxidation [31]. Jager et al. synthesized micro/mesoporous carbide derived carbon powder from Mo_2C using high-temperature chlorination method as a very active catalyst for ORR [32]. Moreover, Stottlemyer and co-workers have demonstrated that transition metal carbides (TMCs) are well suited materials for the electro/-catalysis of oxygen-containing species due to the strong oxygen-carbide interaction [33]. Thus, in recent years, Liao et al. developed a facile calcination method for novel nanoporous molybdenum carbide wires as an active electrocatalyst towards ORR [34].

However, very limited electrocatalytic studies on the in situ formation of β-Mo_2C nanocomposite on graphite carbon using organic amines as reductant and carbon source have been investigated as far as we know. And compared with halides used in rapid solid-state method for the synthesis of carbides previously, oxides are cheaper and more stable in nature. Herein, we successfully prepared β-Mo_2C nanocomposites supported on graphite layers (G-Mo_2C) with the size of Mo_2C nanoparticles ranging from ca. 5 nm to 50 nm, which exhibit considerable activity and superior methanol tolerance during ORR process in alkaline electrolyte. And it is believed that the surrounding graphitic layers works as a protective film on the surface of Mo_2C nanoparticles from being passivated during the ORR operation.

Experimental

All starting materials are of analytical pure grade and arepurchased from commercial sources. Fig 1 shows the typical synthesis process optimized from our previous work beyond the restrictions of evacuating and sealing [35], 0.012 mol melamine and 0.04 mol MoO_3 powder were mixed together, pressed to a pellet and put in an alumina boat. Then, the alumina boat was placed in the center of a horizontal alumina tubular furnace and flushed with nitrogen atmosphere to remove the remaining air in the alumina tube, the furnace temperature was rapidly increased to 1673 K and kept at the peak temperature for 3 hours under N_2 flow at 200 sccm. After the furnace was rapidly cooled to the room temperature in the flow of N_2 atmosphere, the black product was collected from the alumina boat.

Morphology and microstructure of the samples were characterized by TEM (CM200-FEG, Philips), XRD (D/MX-IIIA, RIGAKU) and Raman spectroscopy (INVIA, RENISHAW). Electrochemical characterizations were performed on a CHI660E electrochemical workstation with a three-electrode system consisting of a glassy carbon electrode (5 mm in diameter) loaded with catalysts of 0.5 mg cm^{-2} as the working electrode, a Pt foil as the counter electrode and an Hg/HgO electrode as the reference electrode which was calibrated with respect to reversible hydrogen electrode (RHE) by $E_{(RHE)} = E_{(Hg/HgO)} + 0.92$ V. CV measurements were performed from 0.1 to 0.8 V with a scan rate of 50 mVs^{-1} in N_2- and O_2-saturated 0.1M KOH solution, respectively. Rotating disk electrode (RDE) measurements were conducted at different rotating speed from 400 to 2000 rpm at a scan rate of 5 mv s^{-1} and chronoamperometric responses were

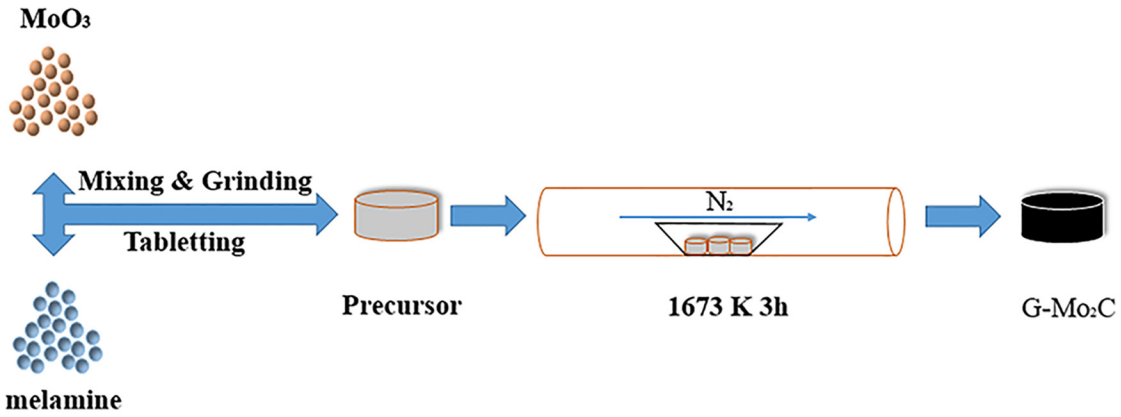

Fig 1. Typical synthesis process of G-Mo_2C nanocomposites.

doi:10.1371/journal.pone.0138330.g001

carried out at a constant voltage of 0.65 V in O_2-saturated 0.1M KOH solution adding 3M methanol at 500 s, successively.

Results and Discussion

As shown in Fig 2, the XRD patterns of the synthesized G-Mo_2C can be typically indexed as the hexagonal-close-packed structure of β-Mo_2C (JCPDS No. 35–0787) together with graphite-2H carbon (JCPDS No. 35–0787). The sharp and strong peaks and highly exposed (101) plane indicate the good crystallization of the Mo_2C nanoparticles while the unobvious diffraction peaks of graphite carbon in the pattern can be attribute to the limited content. It is worth pointing out that the Mo:C ratio of 1:1 and 2:1 in molybdenum carbide crystals are the most stable ones with respect to the stoichiometries. And as for Mo_2C, hexagonal Mo_2C or β-Mo_2C is the

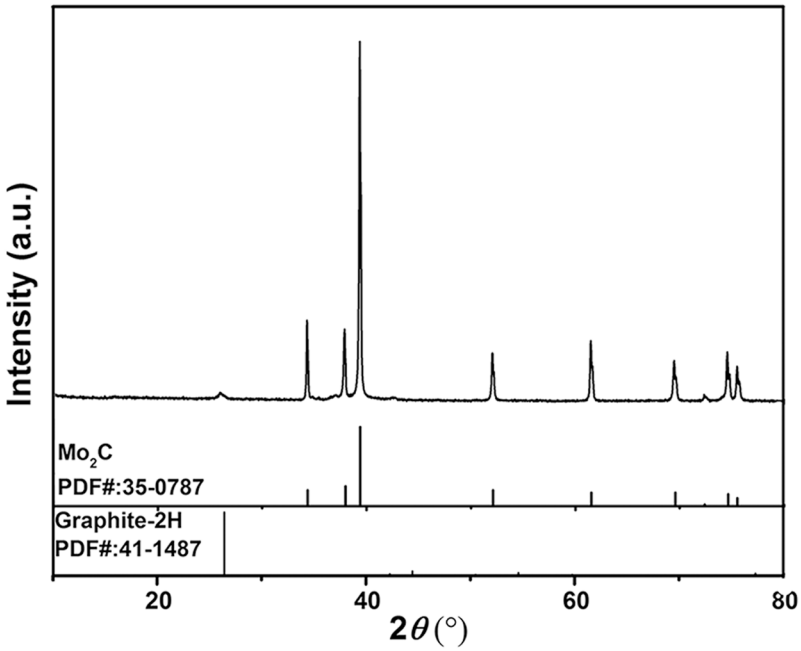

Fig 2. XRD Pattern of G-Mo_2C with the standard diffraction patterns of Graphite and Mo_2C.

doi:10.1371/journal.pone.0138330.g002

high-temperature stable phase with a disordered L'3 structure compared with the low-temperature phase of orthorhombic Mo_2C or α-Mo_2C which adopts an ordered ξ-Fe_2N type structure.

To further investigate the configuration of this novel G-Mo_2C composite, high-resolution transmission electron microscopy (HRTEM) images at different magnification are shown in Fig 3. It can be observed that Mo_2C nanoparticles with sizes ranging from ca. 5 nm to 50 nm anchored on the layers of graphite carbon uniformly corresponding to the results of XRD analysis. Moreover, since the Raman spectroscopy is a powerful and widely used method for the characterization of graphitization degree of carbon-based materials, Raman spectrum of the G-Mo_2C is shown in Fig 4, exhibiting three obvious Raman peaks located at 1355, 1579 and 2695 cm^{-1} which can be attributed to the disorder induced D-band, G-band and 2D-band of crystalline graphite respectively and indicate the existence of the ordered graphitic domains in the G-Mo_2C composites. In addition, the ratio of the G-band to D-band with a value of 1.69 could also be used to judge the high degree of graphitization intuitively [36]. Considering the good contact between graphite carbon layers and β-Mo_2C nanoparticles, the enhanced overall electronic conductivity can be expected to benefit from the functional graphite carbon matrix.

It is reported that the pyrolysis of melamine will first generate NH_3 with a series of intermediate condensed phases such as so-called melam ($(C_3N_3)_2(NH_2)_4(NH)$), melem ($C_6N_7(NH_2)_3$), melon ($(C_6N_7)_3(NH_2)_3(NH)_3$), graphitic carbon nitride materials (g-C_3N_4), and then further release some chemically reactive hydrogen-, carbon-, and nitrogen-containing atomic species such as $C_3N_3^+$, $C_2N_2^+$, $C_3N_2^+$ and CN_2H^+ at higher temperatures [37–40]. Thus, the overall pathway of synthesizing G-Mo_2C can be concluded as follows: MoO_3 is reduced into Mo element by the chemically reactive atomic species with possible low-temperature intermediate phase of Mo_xN, then the as-reduced Mo element is further converted to Mo_2C with the increasing of temperature [35]. Moreover, controlled test of pyrolysis of melamine tablets at same condition was found to obtain no products in the alumina boat, which suggests that the dangling bonds on Mo atom are beneficial to the immobilization of graphite carbon. To further illuminate the chemical interaction between the Mo_2C and graphite carbon, the XPS data of G-Mo_2C in Fig 5 have been provided in consideration of the surface consumption of oxygen on an ORR catalyst. The appearance of surface O species can be ascribed to lattice oxygen in MoO_x due to

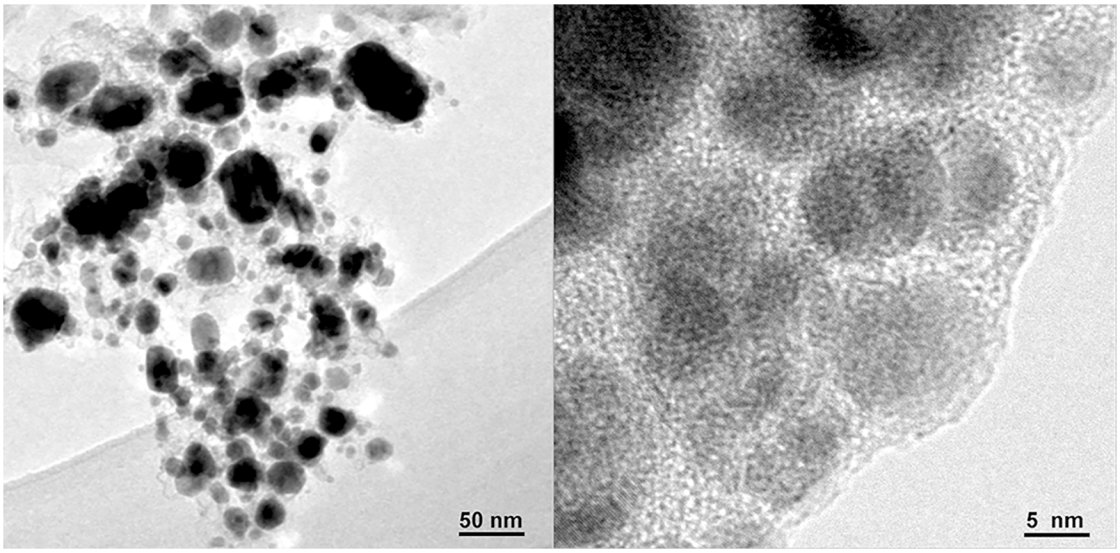

Fig 3. TEM images of G-Mo_2C at different magnifications.

doi:10.1371/journal.pone.0138330.g003

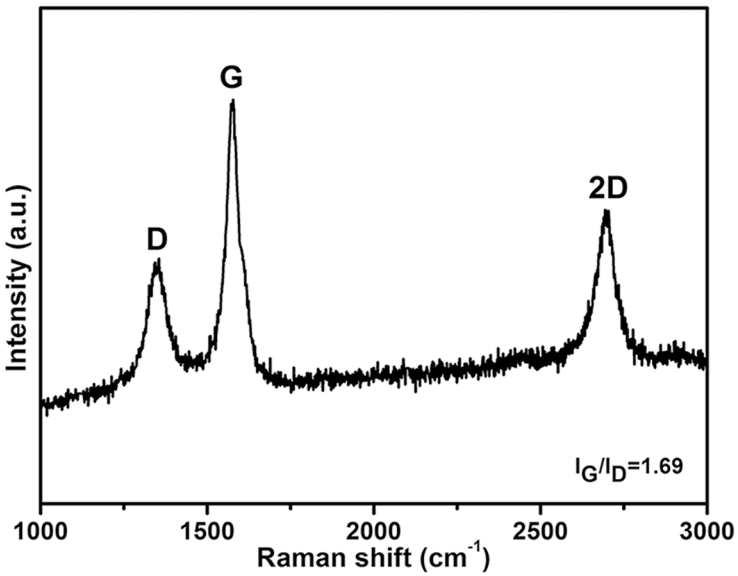

Fig 4. Raman spectrum of graphite in the G-Mo_2C composite.

doi:10.1371/journal.pone.0138330.g004

the ageing process in air [41], and the XPS peaks corresponding to Mo-C-O bond in C 1S and O1S spectra directly prove the chemical interaction [42].

In order to investigate the electrocatalytic performance of the G-Mo_2C composites as a catalyst for the ORR process, CV and RDE methods were employed in 0.1M KOH solution at room temperature. As shown in Fig 6, G-Mo_2C electrode is featureless in the N_2-saturated KOH solution during the CV operation, however obvious ORR peak turns up in O_2-saturated condition suggesting G-Mo_2C as a suitable catalyst for ORR to some extent. Moreover, the ORR activity of G-Mo_2C upon mass transfer was further investigated by the RDE measurements with a fixed potential scan rate of 5 mV s^{-1} by increasing the rotation rate from 400 to 2000 rpm as shown in Fig 7. It is clear that the onset potential is about 0.75 V vs RHE and the diffusion current densities are enhanced with the increase of the rotation rate, and the current density at 1600 rpm is about 3.32 mA cm^{-2} at the potential value of 0.1 V. Obviously, there are two reduction peaks at 0.62 V and 0.54 V instead of a steady diffusion current density, indicating a two steps ORR mechanism for G-Mo_2C.

It is well known to all, there are two major pathways for the reduction of oxygen in alkaline aqueous solution: direct 4-electron pathway to H_2O and 2-electron pathway with "peroxide" as the reduction product. Thus, ORR kinetics determined by the transferred electron number with G-Mo_2C as the catalyst are further studied using Koutecky-Levich (K-L) plots according to the parameters reported by Wang and Jirkovsky [43,44]:

$$\frac{1}{J} = \frac{1}{J_K} + \frac{1}{J_L} = \frac{1}{J_K} + \frac{1}{B\omega^{\frac{1}{2}}} \quad (1)$$

$$B = 0.2nFCD^{\frac{2}{3}}v^{-\frac{1}{6}} \quad (2)$$

Where J and J_K are the measured and kinetic-limiting current densities, ω is the rotation speed (rpm), n is the transferred electron number, F is the Faraday constant (F = 96485 C mol^{-1}), C is the concentration of O_2 in 0.1 M KOH solution ($C = 1.2\times10^{-6}$ mol cm^{-3}), D is the diffusion coefficient of O_2 ($D = 1.9\times10^{-5}$ cm^2 s^{-1}), v is the kinematic viscosity (v = 0.01 cm^2 s^{-1}). As

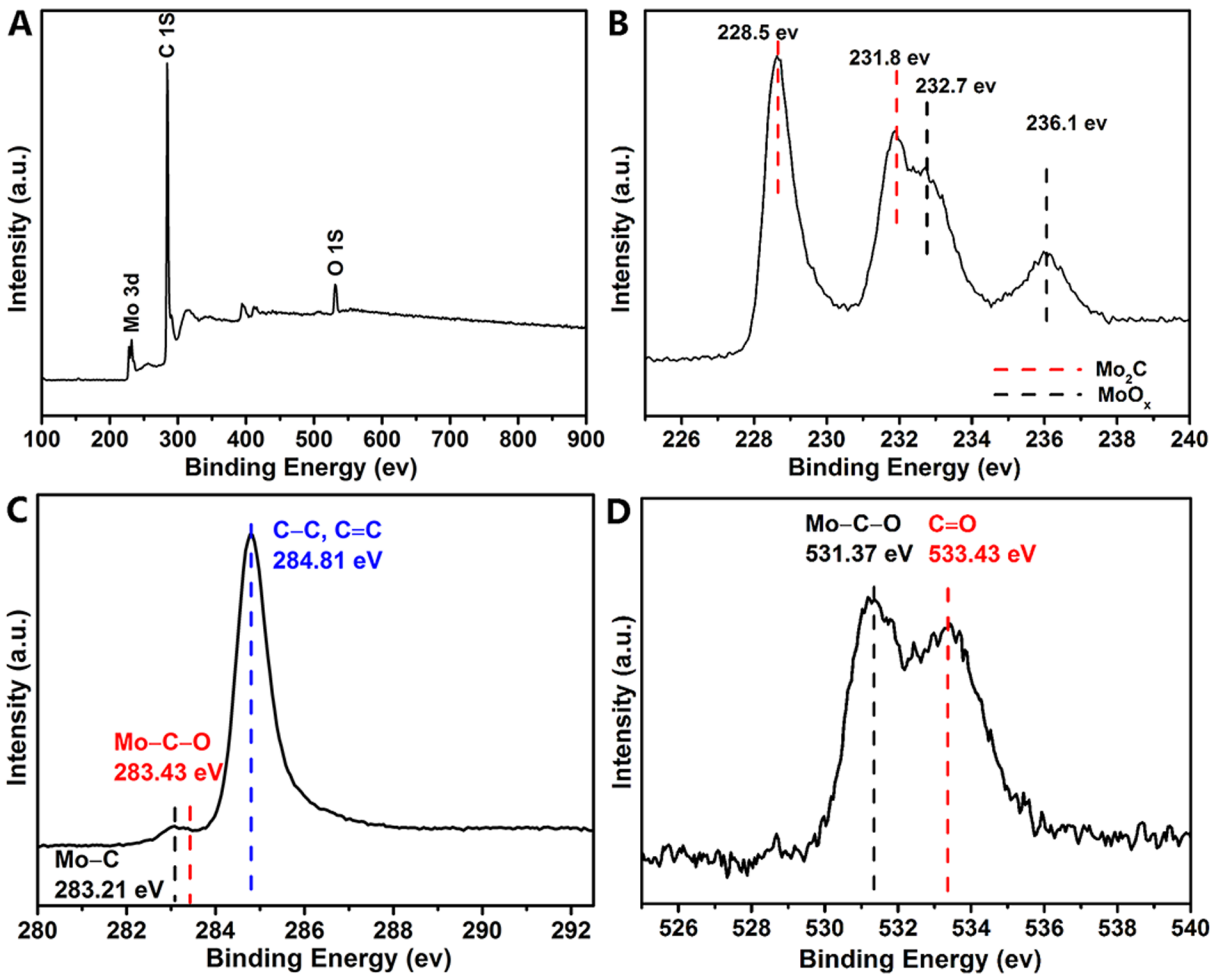

Fig 5. XPS spectra of G-Mo_2C (A)survey; (B) Mo 3d; (C) C 1s and (D) O 1s.

doi:10.1371/journal.pone.0138330.g005

shown in Fig 8, the numbers of electrons transferred for ORR per oxygen molecule during ORR over the potential rangefrom 0.55 to 0.10 V in the illustration increase from 2.13 to 3.21, suggesting the two steps of ORR process are the reduction of O_2 to HO_2^- and then O_2 or HO_2^- to OH^-. Moreover, the ring-disk electrochemistry has also been provided to back up the Koutecky-Levich data in Fig 9, where the oxidation current peaks located at about 0.53 V Vs. RHE can be regarded as the typical detection of HO_2^- intermediate.

According to the calculations of atomic and electronic structure of molybdenum carbide phases and the adsorption and dissociation of molecular oxygen of TMCs by Illas and co-workers [45,46], β-Mo_2C has a strong metallic character and low work function of low Miller-index surface resulting in the fact that O_2 may either bridge two Mo atoms or attach on the top of a Mo surface atom preferably. Thus, Mo_2C itself as well as molybdenum oxides/oxycarbide species can act as catalytic sites for the ORR after the activation of Mo_2C. Furthermore, as a result of the approximate 2-electron reduction process for a large range of potential, G-Mo_2C has a very possible application in the reaction of H_2O_2 electro-generation. However, the ORR catalytic behavior of G-Mo_2C is inferior to the reported work by Liao [34], even comparing with the pure nanoporous molybdenum carbide wires (NP-Mo_2C). Possible reasons can be attributed to the facile mass transport and charge transfer of NP-Mo_2C with the aid of 1-D ordered

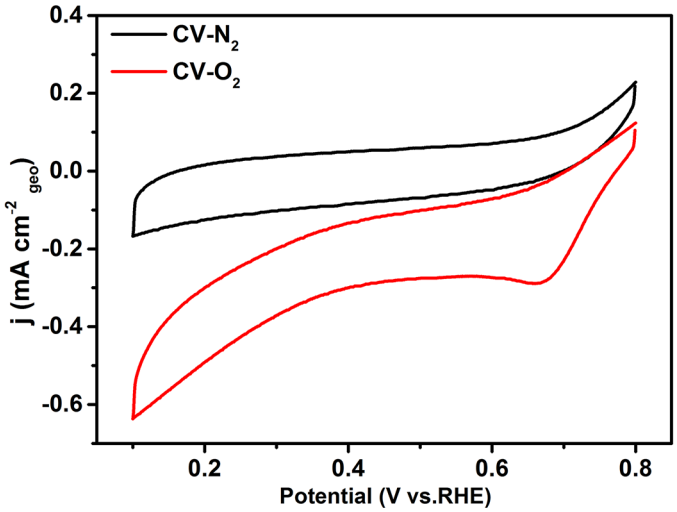

Fig 6. Cyclic voltammetry curves of G-Mo_2C as ORR catalyst in N_2-saturated and O_2-saturated 0.1 M KOH.

doi:10.1371/journal.pone.0138330.g006

structure and intensive nanoporous channels. Further improvement for G-Mo_2C as ORR catalysts can be realized by supporting the nanoparticles of Mo_2C on porous carbon materials as well as reducing the size of Mo_2C nanoparticles.

What's more, considering the methanol crossover issue in the commercialization of alkaline direct methanol fuel cells, the chronoamperometric responses of G-Mo_2C electrode compared with commercial Pt/C upon adding 3M methanol are shown in Fig 10. It is clear that the G-Mo_2C electrode shows negligible change in its ORR current density after the addition of methanol at 500 s, while an instantaneous current jump is observed for Pt/C electrode contributing to the initiation of methanol oxidation reaction (MOR) [47]. The different responses

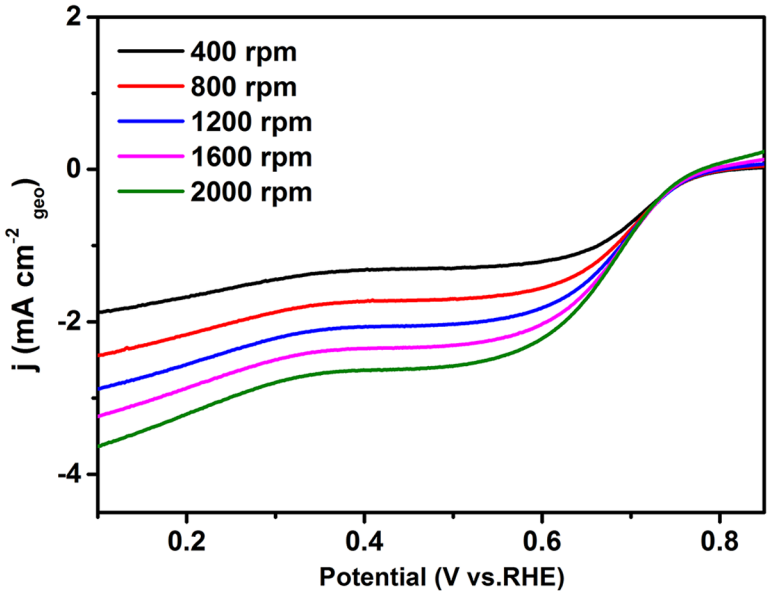

Fig 7. Linear sweep voltammogram of G-Mo_2C as ORR catalysts in O_2-saturated 0.1M KOH, Scan rate: 5 mV s^{-1}.

doi:10.1371/journal.pone.0138330.g007

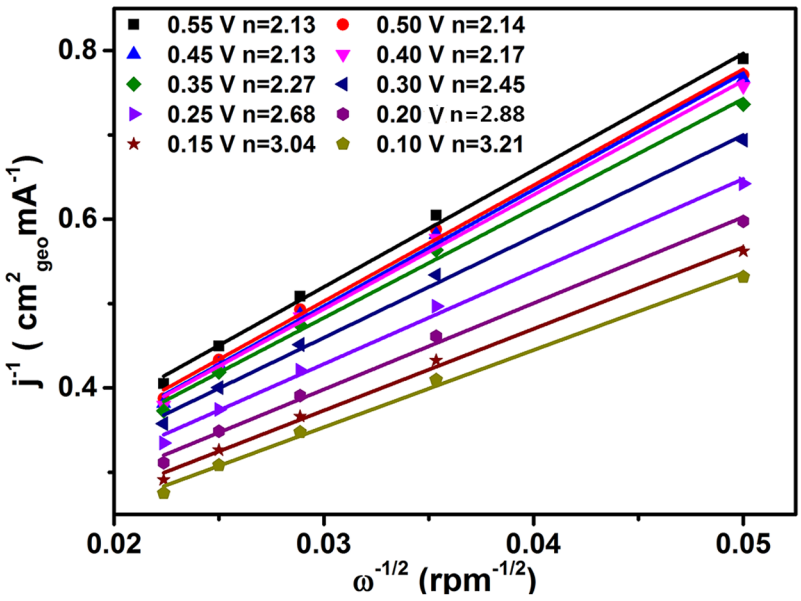

Fig 8. Corresponding K-L plots at different potentials for G-Mo_2C electrode.

doi:10.1371/journal.pone.0138330.g008

demonstrate the remarkably superior methanol tolerance and high catalytic selectivity against methanol of G-Mo_2C to commercial Pt/C as the ORR catalyst. It is believed that the superior methanol tolerance of G-Mo_2C can be attributed to the structure and crystal phase stability of β-Mo_2C with the addition of protective effect of graphite layers, since Mo_2C alone hardly has electrocatalytic effect on methanol oxidation [31]. In addition, the limited degeneration of current density in the following period also indicates the good stability of as-prepared G-Mo_2C nanocomposites.

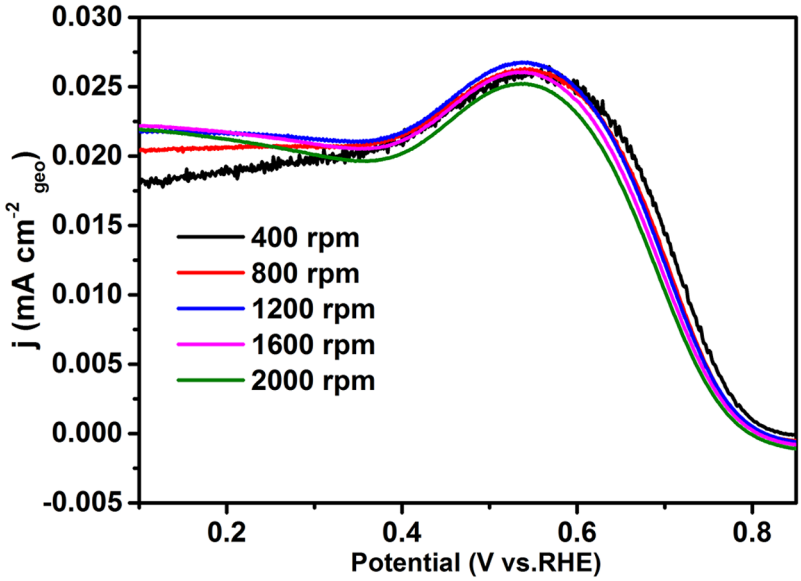

Fig 9. The ring current densities at different rotation rates by RRDE in O_2-saturated 0.1 M KOH at a scan rate of 5 mV s^{-1}.

doi:10.1371/journal.pone.0138330.g009

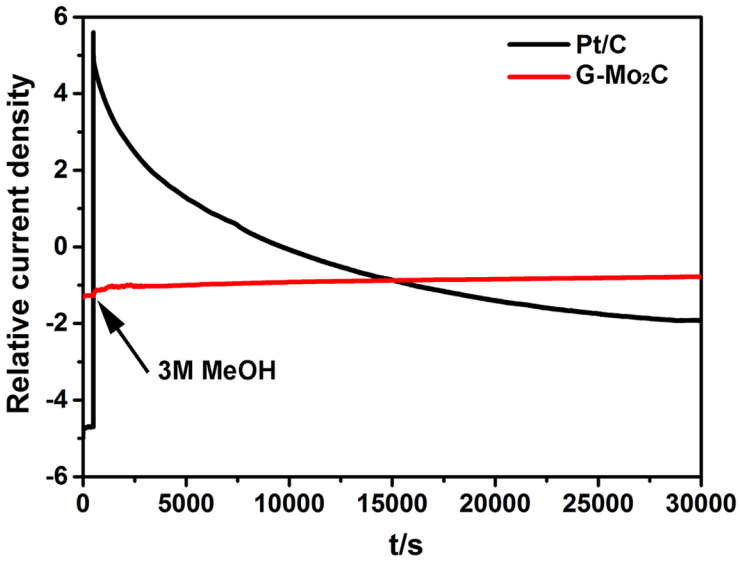

Fig 10. The chronoamperometric responses of Pt/C and G-Mo_2C electrodes adding 3 Mmethanol after 500 s at 0.65 V in O_2-saturated 0.1 M KOH at1600 rpm.

doi:10.1371/journal.pone.0138330.g010

Conclusion

As a summary, novel graphite-Mo_2C nanoparticles composites are synthesized by a single-step solid state reaction route. The morphology and component are further characterized by TEM, XRD and Raman, suggesting that Mo_2C nanoparticles have a uniform distribution on the supported graphite layers. Moreover, G-Mo_2C composites exhibit considerable electrocatalytic performances with certain activity and superior methanol tolerance for ORR in alkaline electrolyte due to the chemical interaction between the protected carbide nanoparticles and activated graphite layers.

Author Contributions

Conceived and designed the experiments: KH WJW ML. Performed the experiments: KH KB CL SL. Analyzed the data: KH RZ DYF YGW TZY ML. Contributed reagents/materials/analysis tools: KH ML JL. Wrote the paper: KH ML.

References

1. Xia BY, Ng WT, Wu HB, Wang X, Lou XW (2012) Self-supported interconnected Pt nanoassemblies as highly stable electrocatalysts for low-temperature fuel cells. Angew. Chem. Int. Edit. 51:7213–7216.
2. Lei M, Li PG, Li LH, Tang WH (2011) A highly ordered Fe-N-C nanoarray as a non-precious oxygen-reduction catalyst for PEM fuel cells. J. Power Sources 196:3548–3552.
3. Liang C, Li JS, Tang HL, Zhang HJ, Zhang HN, Pan M (2014) Approaching high temperature performance for proton exchange membrane fuel cells with 3D ordered silica/Cs2.5H0.5PW electrolytes. J. Mater. Chem. A2:753–760.
4. Li JR, Tang HL, Chen LT, Chen R, Pan M, Jiang SP (2013) Highly ordered and periodic mesoporous Nafion membranes via colloidal silica mediated self-assembly for fuel cells. Chem. Commun. 49 6537–6539.
5. Chen R, Wang ZB, Liang C, Pan M, Tang HL (2013) Promoting electrochemical performance of fuel cells by heteropolyacid incorporated three-dimensional ordered Nafion electrolyte. Sci. Adv. Mater. 5:1788–1795.
6. Cheng FY, Chen J (2012) Metal-air batteries: from oxygen reduction electrochemistry to cathode catalysts. Chem. Soc. Rev. 41:2172–2192. doi: 10.1039/c1cs15228a PMID: 22254234

7. Hardin WG, Slanac DA, Wang X, Dai S, Johnston KP, Stevenson KJ (2013) Highly active, nonprecious metal perovskite electrocatalysts for bifunctional metal-air battery electrodes. J. Phys. Chem. Lett. 4:1254–1259. doi: 10.1021/jz400595z PMID: 26282138
8. Cao RG, Lee JS, Liu ML, Cho J (2012) Recent progress in non-precious catalysts for metal-air batteries. Adv. Energy. Mater. 2:816–829.
9. Huang K, Bi K, Liang C, Lin S, Zhang R, Wang WJ, et al. (2015) Novel VN/C nanocomposites as methanol-tolerant oxygen reduction electrocatalyst in alkaline electrolyte. Sci. Rep. 5:11351. doi: 10.1038/srep11351 PMID: 26100367
10. Lei M, Wang ZB, Li JS, Tang HL, Liu WJ, Wang YG (2014) CeO_2 nanocubes-graphene oxide as durable and highly active catalyst support for proton exchange membrane fuel cell. Sci. Rep. 4:7415. doi: 10.1038/srep07415 PMID: 25491655
11. Lei M, Fu XL, Li PG, Tang WH (2011) Growth and photoluminescence of zinc blende ZnS nanowires via metalorganic chemical vapor deposition. J. Alloy Compd. 509:5769–5772.
12. Lei M, Song B, Guo X, Guo YF, Li PG, Tang WH (2009) Large-scale AlN nanowires synthesized by direct sublimation method. J. Eur. Ceram. Soc. 29:195–200.
13. Zhao HZ, Lei M, Chen XL, Tang WH (2006) Facile route to metal nitrides through melamine and metal oxides. J. Mater. Chem. 16:4407–4412.
14. Song B, Li H, Bao HQ, Lei M, Chen XL, Jian JK (2008) New experimental evidence for origin of ferromagnetism ordering in Fe-doped SiC. Physica B, 403: 2897–2901.
15. Song B, Jian JK, Wang G, Lei M, Xu YP, Chen XL (2007) Facile and general route to nitrides by a modified solid-state metathesis pathway. Chem. Mater. 19:1497–1502.
16. Uhm S, Jeong B, Lee J (2011) A facile route for preparation of non-noble CNF cathode catalysts in alkaline ethanol fuel cells. Electrochim. Acta 56:9186–9190.
17. Yang W, Chen SZ, Lin WM (2012) Oxygen reduction on non-noble metal electrocatalysts supported on N-doped carbon aerogel composites. Int. J. Hydrogen. Energ. 37:942–945.
18. Wang JT, Li S, Zhu GW, Zhao W, Chen RX, Pan M (2013) Novel non-noble metal electrocatalysts synthesized by heat-treatment of iron terpyridine complexes for the oxygen reduction reaction. J. Power Sources 240:381–389.
19. Yang YQ, Wang J, Zheng JF, Li SH, Zhang SB (2014) A stable anion exchange membrane based on imidazolium salt for alkaline fuel cell. J. Membrane Sci. 467:48–55.
20. Ren XM, Price SC, Jackson AC, Pomerantz N, Beyer FL (2014) Highly conductive anion exchange membrane for high power density fuel-cell performance. Acs Appl. Mater. Inter. 6:13330–13333.
21. Pandey RP, Thakur AK, Shahi VK (2014) Stable and efficient composite anion-exchange membranes based on silica modified poly(ethyleneimine)-poly(vinyl alcohol) for electrodialysis. J. Membrane Sci. 469:478–487.
22. Lin BC, Chu FQ, Ren YR, Jia BP, Yuan NY, Shang H et al. (2014) Alkaline stable C2-substituted imidazolium-based cross-linked anion exchange membranes for alkaline fuel cell applications. J. Power Sources 266:186–192.
23. Tuci G, Zafferoni C, Rossin A, Milella A, Luconi L, Innocenti M et al. (2014) Chemically functionalized carbon nanotubes with pyridine groups as easily tunable N-decorated nanomaterials for the oxygen reduction reaction in alkaline medium. Chem. Mater. 26:3460–3470.
24. Lin L, Li M, Jiang LQ, Li YF, Liu DJ, He XQ et al. (2014) A novel iron (II) polyphthalocyanine catalyst assembled on graphene with significantly enhanced performance for oxygen reduction reaction in alkaline medium. J. Power Sources 268:269–278.
25. Kong AG, Zhu XF, Han Z, Yu YY, Zhang YB, Dong B et al. (2014) Ordered hierarchically micro- and mesoporous Fe-N-x-embedded graphitic architectures as efficient electrocatalysts for oxygen reduction reaction. Acs Catal. 4:1793–1800.
26. Tominaga H, Aoki Y, Nagai M (2012) Hydrogenation of CO on molybdenum and cobalt molybdenum carbides. Appl. Catal. A-Gen. 423–424:192–204.
27. Cheekatamarl PK, Thomson WJ (2006) Catalytic activity of molybdenum carbide for hydrogen generation via diesel reforming. J. Power Sources 158:477–484.
28. Cheekatamarla PK, Thomson WJ (2005) Poisoning effect of thiophene on the catalytic activity of molybdenum carbide during tri-methyl pentane reforming for hydrogen generation. Appl. Catal. A-Gen. 287:176–182.
29. Wan C, Regmi YN, Leonard BM (2014) Multiple phases of molybdenum carbide as electrocatalysts for the hydrogen evolution reaction. Angew. Chem. Int. Edit. 53:6407–6410.

30. Ma YF, Guan GQ, Phanthong P, Hao XG, Huang W, Tsutsumi A et al. (2014) Catalytic activity and stability of nickel-modified molybdenum carbide catalysts for steam reforming of methanol. J. Phys. Chem. C118:9485–9496.

31. Yan ZX, Wang HE, Zhang MP, Jiang ZF, Jiang TS, Xie JM (2013) Pt supported on Mo_2C particles with synergistic effect and strong interaction force for methanol electro-oxidation. Electrochim. Acta 95:218–224.

32. Jager R, Kasatkin PE, Hark E, Lust E (2013) Oxygen reduction on molybdenum carbide derived micro-mesoporous carbon electrode in alkaline solution. Electrochem. Commun. 35:97–99.

33. Stottlemyer AL, Kelly TG, Meng Q, Chen JG (2012) Reactions of oxygen-containing molecules on transition metal carbides: surface science insight into potential applications in catalysis and electrocatalysis. Surf. Sci. Rep. 67:201–232.

34. Liao L, Bian XJ, Xiao JJ, Liu BH, Scanlon MD, Girault HH (2014) Nanoporous molybdenum carbide wires as an active electrocatalyst towards the oxygen reduction reaction. Phys. Chem. Chem. Phys. 16:10088–10094. doi: 10.1039/c3cp54754j PMID: 24519082

35. Lei M, Zhao HZ, Yang H, Song B, Cao LZ, Li PG et al. (2008) Syntheses of metal nitrides, metal carbides and rare-earthmetal dioxymonocarbodiimides from metaloxides and dicyandiamide. J. Alloy. Compd. 460:130–137.

36. Peng T, Lv HF, He DP, Pan M, Mu SC (2014) Nano conductive ceramic wedged graphene composites as highly efficient metal supports for oxygen reduction. Sci. Rep-Uk. 4:3968.

37. Jurgens B, Irran E, Senker J, Kroll P, Muller H, Schnick W (2003) Melem (2,5,8-Triamino-tri-s-triazine), an important intermediate during condensation of melamine rings to graphitic carbon nitride: synthesis, structure determination by x-ray powder diffractometry, solid-state NMR, and theoretical studies. J. Am. Chem. Soc. 125:10288–10300. PMID: 12926953

38. Khabashesku VN, Zimmerman JL, Margrave JL (2000) Powder synthesis and characterization of amorphous carbon nitride. Chem. Mater. 12:3264–3270.

39. Gillan EG (2000) Synthesis of nitrogen-rich carbon nitride networks from an energetic molecular azide precursor. Chem. Mater. 12:3906–3912.

40. Lotsch BV, Schnick W (2005) Thermal conversion of guanylurea dicyanamide into graphitic carbon nitride via prototype CN_x precursors. Chem. Mater. 17:3976–3982.

41. Kartachova O, Chen Y, Jones R, Chen YH, Zhang HZ, Glushenkov AM (2014) Evolution of the electrochemical capacitance of transition metal oxynitides with time: the effect of ageing and passivation. J. Mater. Chem. A2:12940–12951.

42. Savinelli R, Li J, Seshadri R, Scott SL (2009) Molybdenum carbide and oxycarbide hydrogen production catalysts: preparation, characterization, and evaluation. 21st NAM P-W-68.

43. Wang SY, Yu DS, Dai LM (2011) Polyelectrolyte functionalized carbon nanotubes as efficient metal-free electrocatalysts for oxygen reduction. J. Am. Chem. Soc. 133:5182–5185. doi: 10.1021/ja1112904 PMID: 21413707

44. Jirkovsky JS, Halasa M, Schiffrin DJ (2010) Kinetics of electrocatalytic reduction of oxygen and hydrogen peroxide on dispersed gold nanoparticles. Phys. Chem. Chem. Phys. 12:8042–8053. doi: 10.1039/c002416c PMID: 20505889

45. Politi JRD, Viñes F, Rodriguez JA, Illas F (2013) Atomic and electronic structure of molybdenum carbide phases: bulk and low miller-index surfaces. Phys. Chem. Chem. Phys. 15:12617–12625. doi: 10.1039/c3cp51389k PMID: 23787949

46. Viñes F, Sousa C, Illas F (2007) A systematic density functional study of molecular oxygen adsorption and dissociation on the (001) surface of group IV-VI transition metal carbides. J. Phys. Chem. C111:16982–16989.

47. Lei M, Wang J, Li JR, Wang YG, Tang HL, Wang WJ (2014) Emerging methanol-tolerant AlN nanowire oxygen reduction electrocatalyst for alkaline direct methanol fuel cell. Sci. Rep-Uk. 4:6013.